

Machine Learning-Based b-Jet Tagging in pp Collisions at $\sqrt{s} = 13$ TeV

Hadi Hassan^{1,*}, Neelkamal Mallick^{1,†} and D.J. Kim^{1,2‡}

¹*University of Jyväskylä, Department of Physics,*

P.O. Box 35, FI-40014 University of Jyväskylä, Finland and

²*Helsinki Institute of Physics, P.O.Box 64, FI-00014 University of Helsinki, Finland*

(Dated: June 8, 2025)

Studying heavy-flavor jets in pp collision is important since they can test pQCD calculations and be used as a reference for heavy-ion collisions. Jets in this analysis are reconstructed from charged particles using the anti- k_T algorithm with a resolution parameter $R = 0.4$ and with pseudorapidity $|\eta| < 0.5$. Beauty jets are tagged using a machine learning model that uses a convolutional neural network trained on information extracted from the jet, tracks, and secondary vertices. The results show that this model is superior compared to other traditional tagging methods.

I. INTRODUCTION

Heavy-Flavor (HF) jets are important for the understanding of quantum chromodynamic (QCD) [1]. They can provide tests for pQCD calculation and have a large mass that acts as a hard scale that suppresses soft-gluon radiations at small angles [2, 3]. They are produced very early in the collision to carry information on the hard collision and information about the high-energy-density medium produced in heavy-ion collisions [4, 5].

Identification of jets formed from hadronization of the heavy b-quarks, so-called "b-jets", is important for measurements like cross section [6–8], fragmentation, and substructure [9, 10], and for understanding the quark-gluon plasma (QGP) in heavy-ion collisions [11, 12].

Various tagging algorithms have been developed to achieve the identification. The problem with traditional b-jet tagging algorithms, such as impact parameter (IP) or secondary vertex (SV) methods [7, 13–15] that rely on a long lifetime of the b-hadron, is that they rely on cuts posed on single variables. Machine learning (ML) methods can combine several parameters from different levels, like tracks, jets, or secondary vertices, and extract complex multidimensional correlations and patterns among the event characteristics. Previous studies from ATLAS and CMS experiments show that the ML models are superior compared to the traditional methods in terms of performance [16–19].

In this paper, Pythia8 Monte Carlo (MC) generator is used [20, 21], mainly since it is widely used and carefully validated by the LHC experiments [22, 23]. Real experimental measurements, such as those performed by ALICE, are affected by finite tracking and pointing resolutions and acceptance, and detector efficiency corrections. Although we present analysis methods that can be optimized for the ALICE environment, we wish to keep the discussion at the methodological level. Hence, we do not perform a complete Monte Carlo (MC) simulation of

the ALICE detector [24] using GEANT4 [25], but instead smear the transverse momentum (p_T) and distance to the closest approach (DCA) distributions to mimic realistic experimental conditions in ALICE.

This paper is organized as follows. Sec. II describes the event generation, spectra smearing, jet reconstruction, feature extraction, and machine learning (ML) methodology. Section III presents the performance of the ML algorithm for the tagging of beauty jets and compares it with traditional methods such as the secondary vertex (SV) and impact parameter methods. And finally Sec. IV summarizes the findings of this analysis.

II. METHODOLOGY

A. Event generation and jet reconstruction

Proton-proton (pp) collision events at center-of-mass energy $\sqrt{s} = 13$ TeV are generated using PYTHIA8 [20, 21] MC event generator with the Monarch 2013 tune [26].

For a more accurate description of the ALICE detector [24] the primary vertex is required to be within $|z| < 10$ cm in the beam direction and only final state (after parton showers and hadronization and decays) charged particles with transverse momentum $p_T > 0.15$ GeV/c and restricted to ALICE tracker acceptance $|\eta| < 0.9$ are used in this analysis.

Then a transverse momentum smearing was applied on these tracks based on the ALICE inner tracking system 2 (ITS2) momentum resolution [27] using the equation:

$$\sigma(p_T)/p_T = \sqrt{a^2 + b^2/p_T^2 + c^2 \cdot p_T^2} \quad (1)$$

where $a = 0.005$, $b = 8e-4$ GeV/c, and $c = 0.001$ (GeV/c)⁻¹ are constants that represents the momentum resolution of the ALICE ITS2 detector. In the addition to the p_T smearing, a smearing of the distance of the closest approach (DCA) of the particles with a respect to primary vertex has been applied according to the DCA resolution of the ITS2 detector [27, 28] σ :

$$\sigma(DCA_{xy/z}) (\mu\text{m}) = \sqrt{a^2 + b^2/p_T^2} \quad (2)$$

* Corresponding author: hadi.hassan@cern.ch

† neelkamal.mallick@cern.ch

‡ dong.jo.kim@jyu.fi

where $a = 7$ and $6 \mu\text{m}$, and $b = 23$ and $25 \mu\text{mGeV}/c$ are the constants for the DCA resolution in the transverse plane and z direction, respectively.

After selecting the particles and smearing their p_T and DCA, they are given to jet clustering algorithm. Jets are reconstructed using the anti- k_T jet clustering algorithm [29] in the FastJet package [30] with a resolution parameter $R = 0.4$, which ensures that most of the initial partonic energy is contained inside the jet. The energies of the tracks are combined using the E-recombination scheme, which considers the mass of the particles with the best strategy. It should be noted here that the real mass of the particles has been used for the jet reconstruction.

A jet is classified as a beauty jet (b-jet) if it contains a beauty quark (from the Pythia stack), a charm jet (c-jet) if it contains a charm quark, and a light-flavor jet (lf-jet) if neither quark is present. Jets with beauty quarks coming from gluon splitting are considered as b-jets.

B. Feature extraction

For the machine learning algorithm, several features are extracted from the jet, tracks, and secondary vertices. For jets, the extracted features are the jet transverse momentum p_T , pseudo-rapidity η , azimuthal angle φ , number of track constituents, number of reconstructed secondary vertices (explained later), and the jet mass.

For the constituent of the jet, the extracted features are particle p_T , particle η , the dot product of the momenta of the track and jet, the dot product of the track and the jet divided by the jet momentum, the distance between the track and the jet axis in $\eta - \varphi$ plane calculated as $\Delta R = \sqrt{(\eta_{\text{jet}} - \eta_{\text{track}})^2 - (\varphi_{\text{jet}} - \varphi_{\text{track}})^2}$. In addition, other features such as the signed DCA in the transverse plane (xy), the signed DCA in z direction, and the distance between the track and the closest reconstructed secondary vertex are calculated with the same distance equation mentioned before. The DCA sign is calculated as the sign of the dot product of the jet axis and the DCA vector. Tracks coming from secondary vertices have positive DCA signs due to their long flight distance, while primary tracks coming from the primary vertex could have positive or negative DCA signs. Some of these features extracted from the jet and tracks are very discriminative between the different jet flavors, especially the signed DCA of the track concerning the primary vertex, as seen on Fig 1.

Prior to particle selection, a maximum DCA (in both xy and z) of 1 cm is applied to reject tracks originating from strange particle decays. Since the DCA is the most discriminative observable, the tracks in each jet are sorted in descending order of their signed DCA, and the top 10 tracks are selected as input to the ML model.

Secondary vertices within jets are reconstructed from their constituent tracks. First, a kinematic cut is applied by selecting tracks with transverse momentum (p_T)

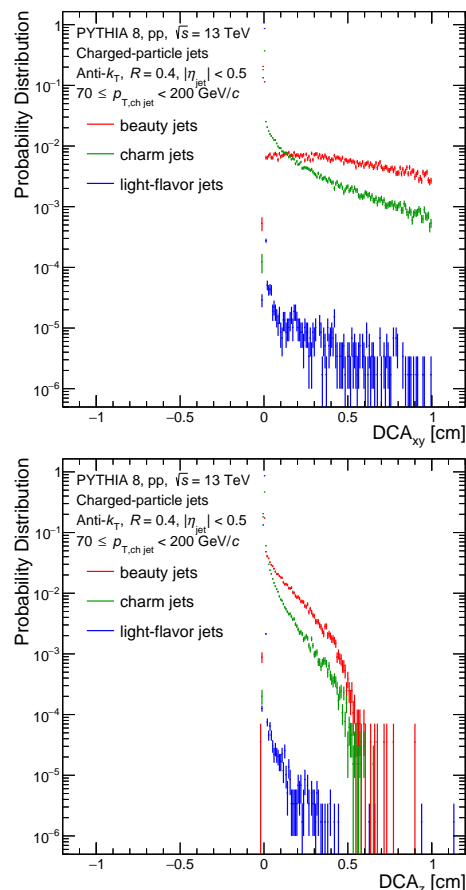


FIG. 1: The transverse (top) and longitudinal (bottom) DCA distributions for different jet flavors.

greater than $0.3 \text{ GeV}/c$, which helps to exclude tracks significantly affected by detector resolution. Triplets of the selected tracks are then combined to identify potential secondary vertices under the assumption that they may originate from a common decay point. For each triplet, a vertex fitting algorithm is employed to determine the optimal vertex position by minimizing the distance between the tracks and the vertex—quantified by the χ^2 fit. The resulting candidate vertices are subjected to additional quality criteria to ensure that only well-reconstructed and physically meaningful secondary vertices are retained. It should be noted here that, there was no smearing done on the secondary vertices since the DCA and momentum of the tracks which are used for the secondary vertex reconstruction are already smeared.

The features from the secondary vertices (SV) reconstructed inside the jet are: SV p_T , η , the distance between the secondary vertex and the jet calculated using the ΔR equation mentioned above, the SV mass, the energy fraction carried by the secondary vertex in the jet, the distance of closest approach in the bending plane of the SV trajectory with respect to the primary vertex, the cosine pointing angle (CPA) which is the cosine of the angle between the SV momentum and the vector pointing

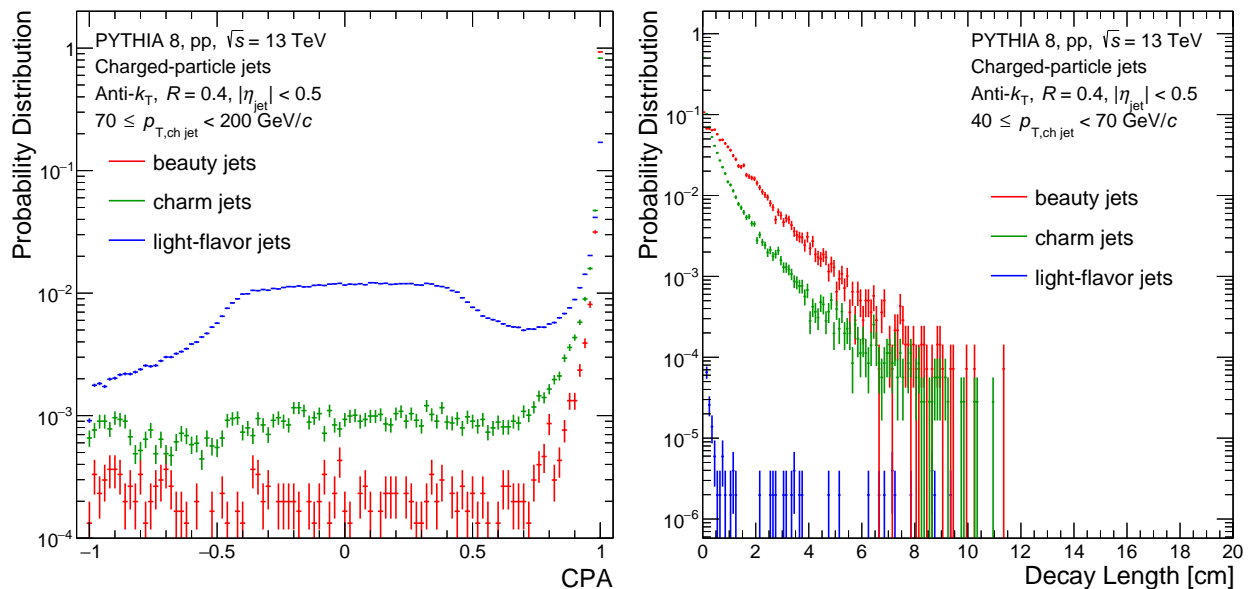


FIG. 2: Left: The cosine pointing angle distribution of the secondary vertices for the different jet flavors. Right: the secondary vertex decay length.

from the PV to SV, χ^2 of the fit of SV reconstruction fit, and the dispersion $D = \sqrt{(d_1^2 + d_2^2 + d_3^2)/N}$ which is the square root of squared summed DCAs of the daughter tracks with respect to the secondary vertex normalized by the number of tracks. In addition to the decay length which is the flight distance between the primary and secondary vertices in the transverse plane and in the z direction.

Figure 2 (right) shows the decay length distribution for the different jet flavors, and Fig. 2 (left) shows the cosine pointing angle distribution for the reconstructed secondary vertex. As can be seen in the figure, the decay length is very discriminative for the different jet flavors.

Since the decay length is the most discriminative feature for secondary vertices, all SVs inside the jets are sorted in descending order based on their decay length. The top 10 SVs are then selected as input for the ML model.

C. Machine learning model

Convolutional neural networks (CNN) [31] are type of neural networks used for image classification by identifying patterns and features. It consists of three types of layers: a convolution layer that applies kernel filters that extract patterns, a pooling layer that reduces the number of inputs, and fully connected layers that will make the final decision and connect the CNN to the output layer. In this analysis, a machine learning algorithm comprised of three branches has been used. Two CNN branches corresponds to the 10 tracks and 10 SVs, and brach the corresponds to the global jet parameters.

The convolution branches consist of 4 convolution lay-

ers made of 64, 32, 32, and 8 filters and one max pooling of 2 (after the first convolution), with 0.2 dropout, 1 stride, same padding, and relu activation function. At the end of the convolution process, the output is flattened. The third branch, which corresponds to the jet features, will be directly concatenated with the two other flattened branches. Then the flattened layer will be connected to 4 fully connected layers with 200, 200, 200, 100 neurons with 0.2 drop out, which in turn will be connected to an output layer with sigmoid activation function. The loss function used is the binary cross entropy with Adam optimizer and a learning rate of 0.001.

In order to train this model, 40M pp collision events at $\sqrt{s} = 13$ TeV are generated using Pythia8. From all of these events we got around 350k b-jets which will be used as signal input for the TensorFlow [32] ML model. The background sample consists of 20% charm jets and 80% light jets, with total number of jets 350k similar to the number of signal jets.

After the model is trained and tested, it was then converted into ONNX [33] format which will be loaded and applied on reconstructed jets when running the event generator.

III. RESULTS

After compiling the model with all its CNN and dense layers, it was trained on sample consisting of 350k beauty jets with batch sizes of 1000 and 300 epochs. Figure 3 (top) shows the receiver operating characteristic (ROC) curve of the ML algorithm. The ROC curve is a graphical representation for the model performance. It shows the true-positive rate (tagged b-jets) versus the false pos-

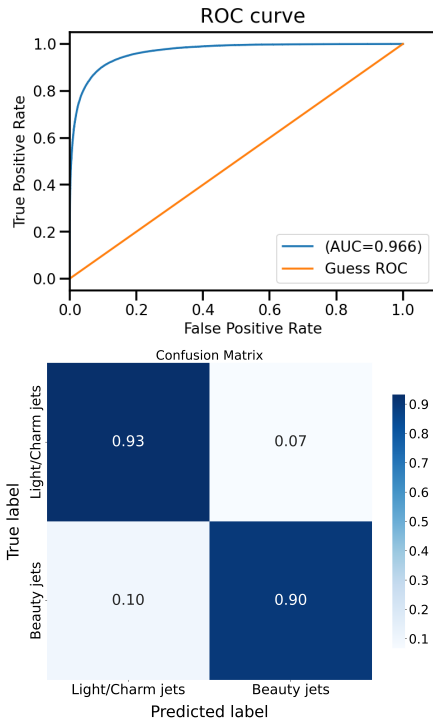


FIG. 3: ROC Curve and Confusion Matrix

itive rate (mistagged c/lf -jets) at various thresholds. As can be seen in the figure, there is a small decrease in b -tagging compared sharp decrease in charm and light-flavor jets. This figure also shows the area under the curve (AUC) which is the area under the ROC curve; if the AUC is 1.0, it means perfect separation between signal and background, while 0.5 means random guessing. The AUC shown in 3 (top) is around 0.966 which is high and shows the strength of the model. Figure 3 (bottom) shows the confusion matrix, which is a table that summarizes the performance of the model by comparing the true labels of jets to the predicted ones. It displays the fraction of correctly classified b , c , and lf -jets and mistakenly identifies b -jets as c/lf -jets and c/lf -jets as b -jets. This misidentification can happen either due to the presence of secondaries in the lf -jets or due to the presence of a displaced secondary vertex in the case of charm jets. The number for the misidentification is very small compared to the number of correctly identified jets, which will reflect the high purity of the tagged jets sample, as will be seen later. Figure 4 (top) shows the $-\ln(1 - \text{score})$ distribution of the different jet flavors, where "score" is the ML evaluation score. The evaluation score is the probability given by the model that a given jet is a b jet. The figure shows that the model's separation power, the distribution decreases sharply for light-flavor jets and more gradually for charm jets. For bottom jets, the distribution exhibits a slow decrease, creating a long tail at higher values.

Figure 4 (bottom) shows the purity versus efficiency of

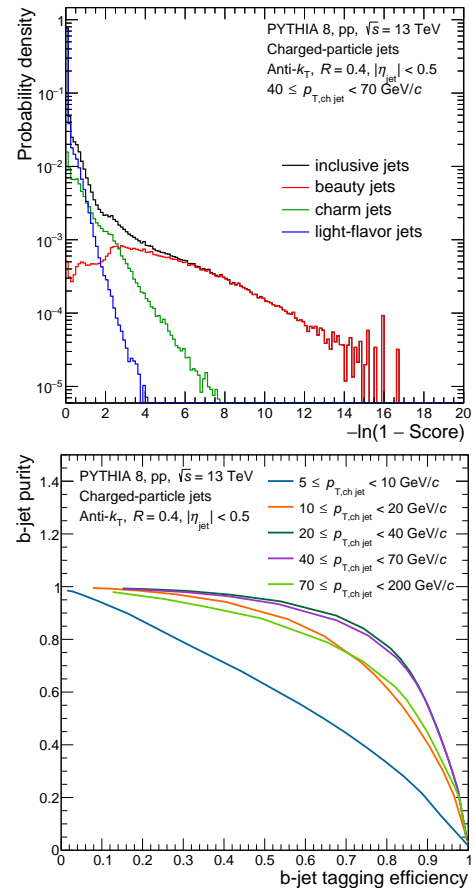


FIG. 4: The logarithmic ML evaluation score distribution for the different jet flavors (top). Bottom, the purity vs tagging efficiency for b -jets from the ML model.

the b tagging model for different jet p_T bins. This figure is crucial since it illustrates the performance of the model in different kinematic regions. It is made by changing the $-\ln(1 - \text{score})$ threshold from 0 to 8.0 and selecting all the jets that passes this threshold. As shown in the figure, low score threshold values will give high efficiencies but low purity since this allows for more background jets to be tagged. Conversely, the high score threshold values lead to lower efficiencies but, in return, give a very high purity since it suppresses large fraction of the background. High efficiency might be needed in measurements that require a maximum signal yield, while purity is crucial for analyses where the background contamination must be minimized, like measuring b jets in Pb-Pb.

When comparing the model performance in the different p_T regions, one can see that the performance is pretty high (it reaches 90% purity at 70% efficiency) for high p_T jets, which is due to the larger DCA of the tracks and the larger decay length of the secondary vertices compared to charm and light jets. The performance at lowest p_T bins is not as good as the high p_T one, which is due to the low particle multiplicity inside the jet compared to

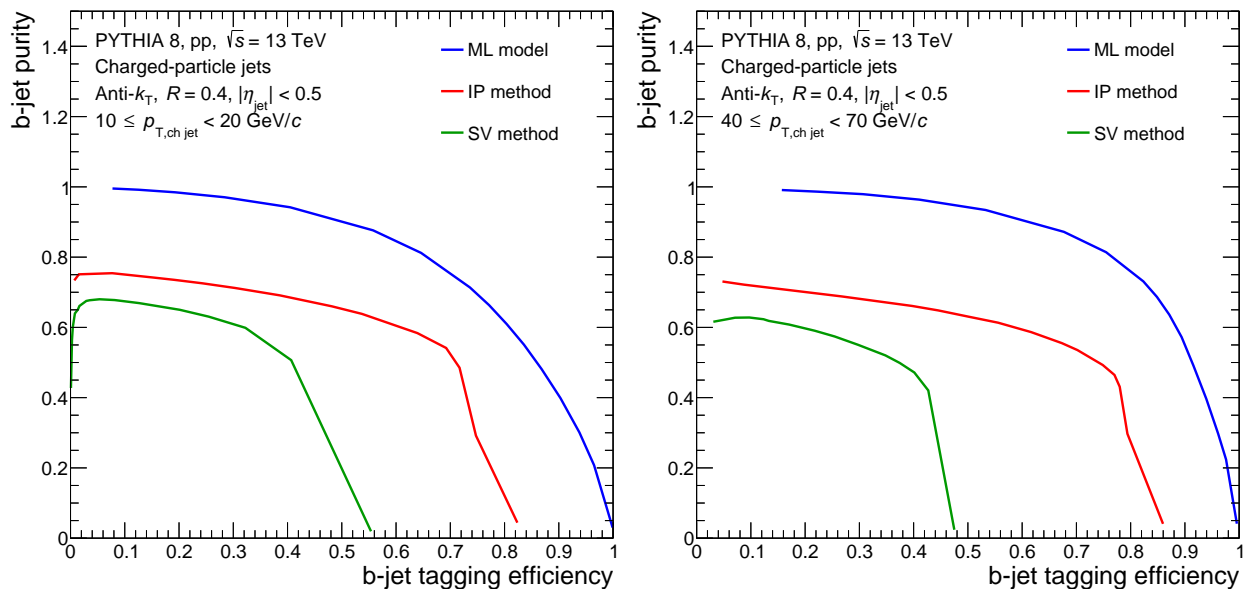


FIG. 5: The ML model performance (purity versus efficiency) compared with the performance of traditional methods (IP and SV methods) in two different p_T ranges.

high p_T jets, also due to the shorter decay lengths which might make the jet resemble charm or light flavor jet.

Figure 5 shows the performance of the ML model compared to traditional cut-based methods like the secondary vertex and the track counting method, which relies on the largest track’s DCA in the jet. These methods are implemented the same way as in [7]. As can be seen, the ML achieves a much higher purity for the same efficiencies, for example, at 50% efficiency, the ML model achieves 30% higher purity compared to the IP method. This means that, the ML model is superior since other methods relies on single observables like the SV decay length or DCA, while the ML fuses all the possible observables from jet, tracks, and secondary vertices. This is a highlight of the advantage of using machine learning.

IV. CONCLUSION

Events in pp collisions at $\sqrt{s} = 13$ TeV have been generated using Pythia8, where charged particle with $p_T > 0.15$ GeV/c and $|\eta| < 0.9$ has been selected. The p_T and DCA of the selected particles are smeared according to the ALICE ITS2 detector transverse momentum and DCA resolutions, respectively. Then, jets are reconstructed from these charged particles using the anti- k_T algorithm with $R = 0.4$. Then a machine learning model that uses CNN has been trained and tested on these jets. The result shows a better performance in terms of purity and tagging efficiency of the ML model compared to the traditional methods.

ACKNOWLEDGMENTS

We would like to thank the Jyväskylä ALICE group for fruitful discussions. We acknowledge CSC—IT Center for Science in Espoo, Finland, for allocating computational resources. NM and DJK are supported by the Academy of Finland through the Center of Excellence in Quark Matter (Grant No. 346328), and HH through Grant No. 346327.

-
- [1] H. D. Politzer, “Asymptotic Freedom: An Approach to Strong Interactions,” *Phys. Rept.* **14** (1974) 129–180.
 [2] Y. L. Dokshitzer, V. A. Khoze, and S. I. Troian, “On specific QCD properties of heavy quark fragmentation (‘dead cone’),” *J. Phys. G* **17** (1991) 1602–1604.
 [3] **ALICE** Collaboration, S. Acharya *et al.*, “Direct

- observation of the dead-cone effect in quantum chromodynamics,” *Nature* **605** no. 7910, (2022) 440–446, [arXiv:2106.05713](https://arxiv.org/abs/2106.05713) [[nuc1-ex](https://arxiv.org/abs/2106.05713)]. [Erratum: *Nature* 607, E22 (2022)].
 [4] B.-W. Zhang, E. Wang, and X.-N. Wang, “Heavy quark energy loss in nuclear medium,” *Phys. Rev. Lett.* **93**

- (2004) 072301, [arXiv:nucl-th/0309040](https://arxiv.org/abs/nucl-th/0309040).
- [5] Y. L. Dokshitzer and D. E. Kharzeev, “Heavy quark colorimetry of QCD matter,” *Phys. Lett. B* **519** (2001) 199–206, [arXiv:hep-ph/0106202](https://arxiv.org/abs/hep-ph/0106202).
- [6] CMS Collaboration, S. Chatrchyan *et al.*, “Inclusive b -Jet Production in pp Collisions at $\sqrt{s} = 7$ TeV,” *JHEP* **04** (2012) 084, [arXiv:1202.4617](https://arxiv.org/abs/1202.4617) [[hep-ex](#)].
- [7] ALICE Collaboration, S. Acharya *et al.*, “Measurement of inclusive charged-particle b -jet production in pp and p -Pb collisions at $\sqrt{s_{NN}} = 5.02$ TeV,” *JHEP* **01** (2022) 178, [arXiv:2110.06104](https://arxiv.org/abs/2110.06104) [[nucl-ex](#)].
- [8] CMS Collaboration, A. Tumasyan *et al.*, “Measurement of the production cross section for $Z+b$ jets in proton-proton collisions at $\sqrt{s} = 13$ TeV,” *Phys. Rev. D* **105** no. 9, (2022) 092014, [arXiv:2112.09659](https://arxiv.org/abs/2112.09659) [[hep-ex](#)].
- [9] CMS Collaboration, A. M. Sirunyan *et al.*, “Measurement of b jet shapes in proton-proton collisions at $\sqrt{s} = 5.02$ TeV,” *JHEP* **05** (2021) 054, [arXiv:2005.14219](https://arxiv.org/abs/2005.14219) [[hep-ex](#)].
- [10] CMS Collaboration, A. Tumasyan *et al.*, “Search for medium effects using jets from bottom quarks in PbPb collisions at $s_{NN}=5.02$ TeV,” *Phys. Lett. B* **844** (2023) 137849, [arXiv:2210.08547](https://arxiv.org/abs/2210.08547) [[hep-ex](#)].
- [11] ATLAS Collaboration, G. Aad *et al.*, “Measurement of the nuclear modification factor of b -jets in 5.02 TeV Pb+Pb collisions with the ATLAS detector,” *Eur. Phys. J. C* **83** no. 5, (2023) 438, [arXiv:2204.13530](https://arxiv.org/abs/2204.13530) [[nucl-ex](#)].
- [12] CMS Collaboration, S. Chatrchyan *et al.*, “Evidence of b -Jet Quenching in PbPb Collisions at $\sqrt{s_{NN}} = 2.76$ TeV,” *Phys. Rev. Lett.* **113** no. 13, (2014) 132301, [arXiv:1312.4198](https://arxiv.org/abs/1312.4198) [[nucl-ex](#)]. [Erratum: *Phys.Rev.Lett.* 115, 029903 (2015)].
- [13] CMS Collaboration, S. Chatrchyan *et al.*, “Identification of b -Quark Jets with the CMS Experiment,” *JINST* **8** (2013) P04013, [arXiv:1211.4462](https://arxiv.org/abs/1211.4462) [[hep-ex](#)].
- [14] ATLAS Collaboration, “Secondary vertex finding for jet flavour identification with the ATLAS detector,” tech. rep., CERN, Geneva, 2017. <https://cds.cern.ch/record/2270366>.
- [15] ATLAS Collaboration, “Optimisation and performance studies of the ATLAS b -tagging algorithms for the 2017-18 LHC run,” tech. rep., CERN, Geneva, 2017. <https://cds.cern.ch/record/2273281>.
- [16] ATLAS Collaboration, G. Aad *et al.*, “Fast b -tagging at the high-level trigger of the ATLAS experiment in LHC Run 3,” *JINST* **18** no. 11, (2023) P11006, [arXiv:2306.09738](https://arxiv.org/abs/2306.09738) [[hep-ex](#)].
- [17] ATLAS Collaboration, G. Aad *et al.*, “ATLAS flavour-tagging algorithms for the LHC Run 2 pp collision dataset,” *Eur. Phys. J. C* **83** no. 7, (2023) 681, [arXiv:2211.16345](https://arxiv.org/abs/2211.16345) [[physics.data-an](#)].
- [18] A. Cagnotta, F. Carnevali, and A. De Iorio, “Machine learning applications for jet tagging in the cms experiment,” *Applied Sciences* **12** no. 20, (2022) . <https://www.mdpi.com/2076-3417/12/20/10574>.
- [19] E. Bols, J. Kieseler, M. Verzetti, M. Stoye, and A. Stakia, “Jet Flavour Classification Using DeepJet,” *JINST* **15** no. 12, (2020) P12012, [arXiv:2008.10519](https://arxiv.org/abs/2008.10519) [[hep-ex](#)].
- [20] T. Sj"strand *et al.*, “An introduction to pythia 8.2,” *Comput. Phys. Commun.* **191** (2015) 159–177.
- [21] C. Bierlich *et al.*, “A comprehensive guide to the physics and usage of PYTHIA 8.3” *SciPost Phys. Codeb.* **2022** (2022) 8, [arXiv:2203.11601](https://arxiv.org/abs/2203.11601) [[hep-ph](#)].
- [22] ALICE Collaboration, S. Acharya *et al.*, “Pseudorapidity distributions of charged particles as a function of mid- and forward rapidity multiplicities in pp collisions at $\sqrt{s} = 5.02, 7$ and 13 TeV,” *Eur. Phys. J. C* **81** no. 7, (2021) 630, [arXiv:2009.09434](https://arxiv.org/abs/2009.09434) [[nucl-ex](#)].
- [23] CMS Collaboration, A. M. Sirunyan *et al.*, “Extraction and validation of a new set of CMS PYTHIA8 tunes from underlying-event measurements,” *Eur. Phys. J. C* **80** no. 1, (2020) 4, [arXiv:1903.12179](https://arxiv.org/abs/1903.12179) [[hep-ex](#)].
- [24] ALICE Collaboration, K. Aamodt *et al.*, “The alice experiment at the cern lhc,” *Journal of Instrumentation* **3** no. 08, (Aug, 2008) S08002. <https://dx.doi.org/10.1088/1748-0221/3/08/S08002>.
- [25] S. Agostinelli *et al.*, “Geant4—a simulation toolkit,” *Nuclear Instruments and Methods in Physics Research Section A: Accelerators, Spectrometers, Detectors and Associated Equipment* **506** no. 3, (2003) 250–303. <https://www.sciencedirect.com/science/article/pii/S0168900203013688>.
- [26] P. Skands, S. Carrazza, and J. Rojo, “Tuning PYTHIA 8.1: the Monash 2013 Tune,” *Eur. Phys. J. C* **74** no. 8, (2014) 3024, [arXiv:1404.5630](https://arxiv.org/abs/1404.5630) [[hep-ph](#)].
- [27] ALICE Collaboration, B. Abelev *et al.*, “Technical Design Report for the Upgrade of the ALICE Inner Tracking System,” tech. rep., 2014. <https://cds.cern.ch/record/1625842>.
- [28] A. S. Triolo and on behalf of the ALICE collaboration, “Calibration and performance of the upgraded alice inner tracking system,” *Journal of Instrumentation* **20** no. 01, (Jan, 2025) C01030. <https://dx.doi.org/10.1088/1748-0221/20/01/C01030>.
- [29] M. Cacciari, G. P. Salam, and G. Soyez, “The anti- k_t jet clustering algorithm,” *JHEP* **04** (2008) 063, [arXiv:0802.1189](https://arxiv.org/abs/0802.1189) [[hep-ph](#)].
- [30] M. Cacciari, G. P. Salam, and G. Soyez, “FastJet User Manual,” *Eur. Phys. J. C* **72** (2012) 1896, [arXiv:1111.6097](https://arxiv.org/abs/1111.6097) [[hep-ph](#)].
- [31] Y. Lecun, L. Bottou, Y. Bengio, and P. Haffner, “Gradient-based learning applied to document recognition,” *Proceedings of the IEEE* **86** no. 11, (1998) 2278–2324.
- [32] TensorFlow Community, “TensorFlow.” <https://www.tensorflow.org/>, 2025.
- [33] ONNX Community, “ONNX: Open Neural Network Exchange.” <https://onnx.ai>, 2025.